Anisotropic optical properties of excitons in strain-controlled InAs quantum dots

H. Tahara, Y. Ogawa, and F. Minami
Department of Physics, Tokyo Institute of Technology, Oh-Okayama 2-12-1, Tokyo 152-8551, Japan

K. Akahane and M. Sasaki
National Institute of Information and Communications Technology, 4-2-1 Nukui-kitamachi, Koganei, Tokyo 184-8795, Japan
(Received 24 October 2012; revised manuscript received 17 December 2012; published 10 January 2013)

We report the optical anisotropy of excitons in self-assembled InAs quantum dots (QDs), the strain of which is controlled by tuning the lattice constant of the spacer layers between stacked QD layers. The strain dependence of the energy structure for excitons is investigated using the four-wave mixing technique. The fine-structure beat and the exciton-biexciton beat in four-wave mixing measurements clearly show that the fine-structure splitting of exciton states increases with increasing strain in the growth plane. The strain also causes significant optical anisotropy, which is observed by the angular-dependent measurements of the collinear polarization of excitation pulses. The strain dependence of the optical anisotropy is accurately reproduced by a model calculation in which the valence band mixing between heavy- and light-hole bands is taken into account. We demonstrate that the optical properties of excitons in QD ensembles are successfully controlled by tuning the lattice constant of the spacer layers.

DOI: 10.1103/PhysRevB.87.035304 PACS number(s): 78.47.nj, 42.50.Md, 78.67.Hc

I. INTRODUCTION

Electrons and holes in semiconductor quantum dots (QDs) construct discrete energy structures. The optical and electronic properties of QDs have attracted considerable attention due to characteristic features induced by the confinement potential in zero-dimensional nanostructures. These carriers in QDs exhibit long coherence times due to their isolation from other carriers; this phenomenon has been widely investigated for control of quantum states.[1–5] Furthermore, the confinement potential creates neutral and charged excitonic complexes including many-particle states, which are not generated in bulk semiconductors.[6–8] The energy structure of QDs varies depending on several factors, and the size and shape dependence of the energy structure has been investigated both experimentally and theoretically.[9–14]

The strain dependence of the energy structure is a topic that is still to be addressed because the strain induced by lattice mismatch is essential for the fabrication of QDs in the Stranski-Krastanov growth mode. The strain causes optical anisotropy of QDs as a result of the valence band mixing between heavy-hole (hh) and light-hole (lh) bands; such mixing has been observed via single-dot spectroscopy.[15–17] The growth technique of QDs is also related closely to the strain. Self-assembled QDs with high density have been fabricated using the stacked structure of QD layers.[18,19] The influence of strain, which is accumulated with the increase in the number of stacked QD layers, is controlled by the spacer layers between the QD layers. Single-dot spectroscopy is a useful technique to study the energy structure in low-density QDs; however, it is quite difficult to investigate the energy structure of high-density QDs in the frequency domain. Instead of the measurements in the frequency domain, four-wave mixing (FWM) measurements in the time domain can provide information regarding the energy structure of QDs. In the FWM measurements, the energy structure has been investigated as quantum beats due to the fine-structure splitting and the biexciton formation.[4,20] In order to control the collective optical properties of highly stacked QDs, it is necessary to examine the influence of spacer layers stacked between QD layers.

In this paper, we examine the strain dependence of optical anisotropy for excitons in self-assembled InAs QDs. The highly stacked QDs exhibit fairly uniform anisotropy depending on the lattice mismatch between the QDs and spacer layers. The strain dependence of the energy structure for excitons has been measured using the FWM technique for collinearly and cocircularly polarized excitations. We have investigated the strain dependence of the dipole moments of excitons by using a model calculation including the mixing of hh and lh excitons due to the strain induced by the spacer layers.

II. EXPERIMENTAL DETAILS

A. Samples

The investigated samples were grown on a InP(311)B substrate by molecular beam epitaxy. These samples contain 60 layers of InAs self-assembled quantum dots separated by 20-nm-thick $In_{1-x-y}Ga_xAl_yAs$ spacers. Highly stacked InAs QDs are realized by the strain-compensation technique.[18,19] In this technique, the spacer layers are fabricated with lattice constants slightly smaller than that of the substrate. Therefore, the spacer layers enable the removal of the strain accumulated in the InAs QD layers, the lattice constant of which is larger than that of the substrate. Tuning the compositions of the spacer layers, we prepared five samples with different lattice constants of spacer layers, which are denoted as S1, S2, S3, S4, and S5. The topographic image of InAs QDs for sample S3 is shown in Fig. 1(a), which is measured using an atomic force microscope. The average lateral sizes of QDs are obtained to be 35 and 51 nm along the $[01\bar{1}]$ and $[\bar{2}33]$ directions, respectively. The average height of QDs is 4.1 nm. The sizes of QDs for the other samples are similar to these values. The lattice constants of these samples a_{spacer} are indicated in Fig. 1(b). The lattice constant a_{spacer} is plotted as a function of

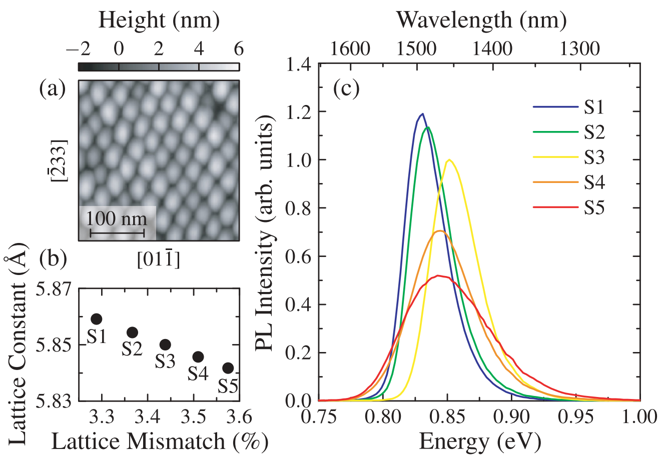

FIG. 1. (Color online) (a) Topographic image of InAs quantum dots. (b) Lattice constant of spacer layers as a function of the lattice mismatch between the InAs quantum dots and spacer layers. (c) Photoluminescence (PL) spectrum of InAs quantum dots at a temperature of 3.4 K. The signals are normalized by the peak intensity of sample S3.

the lattice mismatch between the InAs QDs and spacer layers, and this lattice mismatch is expressed as $(a_{\mathrm{InAs}} - a_{\mathrm{spacer}})/a_{\mathrm{InAs}}$ using the lattice constant of InAs a_{InAs}. The sample S1 was fabricated with the lowest strain in the samples, and the lattice mismatch increases from S1 to S5.

The photoluminescence (PL) of InAs QDs is shown in Fig. 1(c). The PL spectra of the five samples were measured at 3.4 K with an optical pulse excitation of wavelength 800 nm. The wavelength of the emitted light is approximately 1.5 μm for the five samples. The full width at half maximum (FWHM) of the PL spectra increases from S1 to S5. The broad spectral width of the exciton resonance is characterized by variation in the size and shape of QDs. The sample S5 with the highest strain exhibits a FWHM of 77.0 meV, which is twice the FWHM value of 36.7 meV observed in the spectrum of sample S1.

B. Experimental setup

In order to investigate the energy structure of InAs QDs, time-integrated four-wave mixing (TI-FWM) measurements were performed. Optical pulses were generated by an optical parametric oscillator pumped by a mode-locked Ti:sapphire laser tuned to the exciton resonant wavelength of 1470 nm. The pulse duration was 130 fs and the repetition rate was 76 MHz. The first and second excitation pulses were incident on the sample with wave vectors of $\boldsymbol{k}_1$ and $\boldsymbol{k}_2$, respectively. The TI-FWM signal in the direction of $2\boldsymbol{k}_2 - \boldsymbol{k}_1$ was detected by a photodetector in transmission geometry. The samples were mounted in a closed-cycle refrigerator at a temperature of 3.4 K. The FWM measurements were performed for different excitation configurations by changing the polarization of the excitation pulses. In this paper, we use the notations X, Y, and Z for the $[01\bar{1}]$, $[\bar{2}33]$, and [311] directions, respectively. The excitation pulses were set to be collinear and cocircular polarizations in the XY plane. The notations X, D, and Y are used for linear polarization angles of 0°, 45°, and 90°, respectively, in the XY plane, where the angle of linear polarization is measured from the X direction. The right-circularly polarized light is denoted by R for cocircularly polarized excitation.

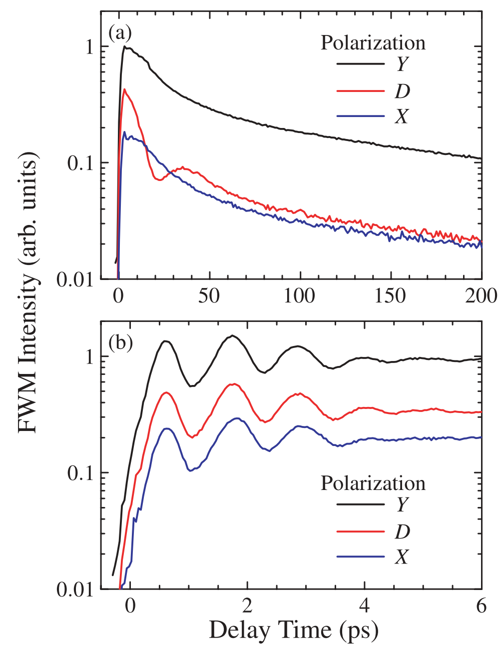

FIG. 2. (Color online) Four-wave mixing intensity for sample S3 at a delay time of (a) 0 to 200 ps and (b) 0 to 6 ps with Y-, D-, and X-polarized excitations.

III. RESULTS AND DISCUSSION

A. Fine-structure beat and exciton-biexciton beat

The TI-FWM signals of sample S3, measured with Y-, D-, and X-polarized excitations, are shown in Figs. 2(a) and 2(b). In Fig. 2(a), a quantum beat is observed for D-polarized excitation; however, it disappears for X- and Y-polarized excitations. This result shows that the exciton states in QDs are characterized by X- and Y-polarized states. In our study, these excitons are called the X and Y excitons, respectively. From the period of the quantum beat, the energy splitting between these states $\hbar\Delta_{XY}$ is obtained to be 87 ± 1 μeV. This so-called fine-structure splitting is caused by the anisotropic confinement potential of QDs in the XY plane; this splitting has been investigated in terms of the long-range electron-hole exchange interaction.[11,12,21,22] In the range from 0 to 6 ps, an exciton-biexciton beat is observed for all linearly polarized excitations as shown in Fig. 2(b). The exciton-biexciton beat is caused by the interference of the signals from the following two transitions: transition from the exciton state to the ground state, and that from the biexciton state to the exciton state. The signal of the biexciton transition is energetically different from that of the exciton transition by the biexciton binding energy $\hbar\Delta_{\mathrm{B}}$. The beat periods for X- and Y-polarized excitations correspond to energy differences of 3.35 ± 0.02 and 3.52 ± 0.02 meV, respectively. The slight difference between these values is explained by the fine-structure splitting between the X and Y excitons.[4,20] As derived in Appendix C, the phase factors $e^{i(\Delta_{\mathrm{B}}-\Delta_{XY})\tau}$ and $e^{i(\Delta_{\mathrm{B}}+\Delta_{XY})\tau}$ express the exciton-biexciton beats for X- and Y-polarized excitations as a function of the delay time τ. The biexciton binding energy $\hbar\Delta_B$ and the fine-structure splitting $\hbar\Delta_{XY}$ are obtained from the relations $\hbar\Delta_B = \hbar(\omega_Y + \omega_X)/2$ and $\hbar\Delta_{XY} = \hbar(\omega_Y - \omega_X)/2$, where the energies of $\hbar\omega_X$ and $\hbar\omega_Y$ are determined from the periods of the exciton-biexciton beat with X- and Y-polarized excitations, respectively. Using these relations, the biexciton binding energy and the fine-structure splitting are obtained to be 3.43 ± 0.01 meV and 83 ± 15 μeV. The value of the fine-structure splitting shows a large error because it is obtained from the slight difference of the beat periods; however, it corresponds to that directly obtained from the fine-structure beat. The fine-structure splitting between the X and Y excitons $\hbar\Delta_{XY}$ is one order of magnitude smaller than the biexciton binding energy $\hbar\Delta_B$. This relation exhibits the difference of observed range of the quantum beats in the time domain.

In order to investigate the strain dependence of the fine-structure splitting and the biexciton binding energy, we measured the quantum beats for the five samples. The fine-structure beat exhibits a damped oscillation due to the inhomogeneous broadening of the fine-structure splitting. The damped quantum beat for D-polarized excitation is expressed as $|1 + C_{XY} e^{i\Delta_{XY}\tau} e^{-(\sigma_{XY}^2/4)\tau^2}|^2$, where C_{XY} denotes the beat amplitude. The inhomogeneous broadening of the fine-structure splitting is assumed as a Gaussian distribution with a central value $\hbar\Delta_{XY}$ and a linewidth $\hbar\sigma_{XY}$. These values are obtained as shown in Figs. 3(a)–3(c). The central value of the fine-structure splitting $\hbar\Delta_{XY}$ increases from 75.8 ± 0.8 μeV to 126 ± 5 μeV with increasing lattice mismatch as shown in Fig. 3(a). This result shows that the anisotropy of the QD confinement potential is increased by the strain induced by the spacer layers. The linewidth $\hbar\sigma_{XY}$ also shows an increasing tendency, corresponding to increase in $\hbar\Delta_{XY}$ [see Fig. 3(b)]. The amplitude of the fine-structure beat between the X and Y excitons is smaller than 1 as shown in Fig. 3(c) because the FWM signal from the X exciton is significantly weaker than that from the Y exciton as shown in Fig. 2(a). To obtain the biexciton binding energy, the exciton-biexciton beat is analyzed using the beat component $|2 - C_B e^{i(\Delta_B - \Delta_{XY})\tau} e^{-(\sigma_B^2/4)\tau^2}|^2$ for X-polarized excitation. The signal for Y-polarized excitation is expressed as this equation by replacing $\Delta_B - \Delta_{XY}$ with $\Delta_B + \Delta_{XY}$. In the equation, the inhomogeneous broadening of the biexciton binding energy is also assumed to be a Gaussian distribution similar to that of the fine-structure splitting. The results for the exciton-biexciton beat are shown in Figs. 4(a)–4(d). The fine-structure splitting in Fig. 4(a), which is obtained from the exciton-biexciton beats, coincides with the results in Fig. 3(a), which are directly measured from the fine-structure beat. The central value of the biexciton binding energy $\hbar\Delta_B$ does not show a clear dependence on lattice mismatch, as observed in Fig. 4(b). However, the inhomogeneous broadening of the binding energy $\hbar\sigma_B$ exhibits a decreasing tendency, as shown in Fig. 4(c). The broad linewidth corresponds to the fast damping of the exciton-biexciton beat in TI-FWM measurements. The linewidth indicates the shape inhomogeneity of QDs in the Z direction because the biexciton binding energy strongly depends on the height of QDs.[13,14] The decreasing tendency shows that the biexciton binding energy relative to the exciton energy becomes more homogeneous with increasing strain. It should be noted that the exciton energy is fixed by the energy of the excitation pulse because FWM signals are generated by resonantly excited excitons. The beat amplitude of the exciton-biexciton beat C_B indicates the ratio of the biexciton excitation in the excited QDs, which is smaller than 1 as shown in Fig. 4(d).

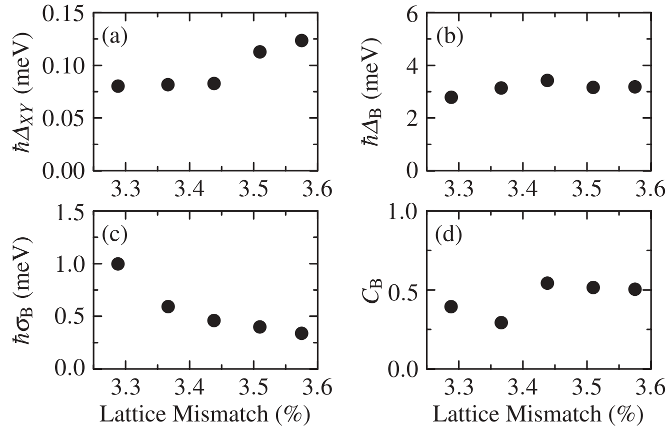

FIG. 4. Strain dependence of (a) fine-structure splitting $\hbar\Delta_{XY}$, (b) biexciton binding energy $\hbar\Delta_B$, (c) inhomogeneous broadening of biexciton binding energy $\hbar\sigma_B$, and (d) beat amplitude C_B. These values are obtained from the exciton-biexciton beats with X- and Y-polarized excitations.

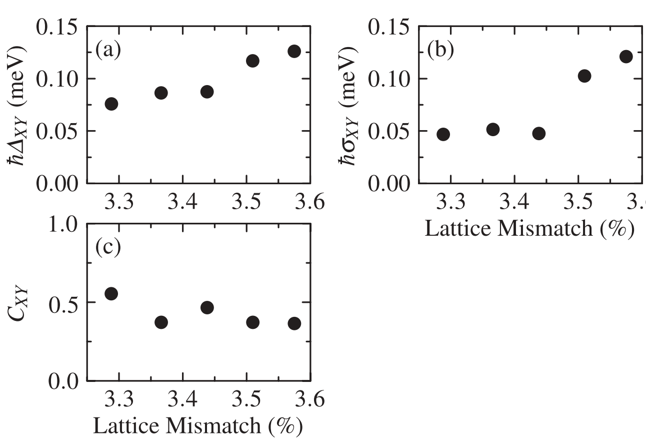

FIG. 3. Strain dependence of (a) fine-structure splitting $\hbar\Delta_{XY}$, (b) inhomogeneous broadening of fine-structure splitting $\hbar\sigma_{XY}$, and (c) beat amplitude C_{XY}. These values are obtained from the fine-structure beat with D-polarized excitation.

B. Angular dependence of anisotropic four-wave mixing intensity for collinearly polarized excitation

As shown in Figs. 2(a) and 2(b), the FWM intensity is significantly changed for X- and Y-polarized excitations. The ratio of these FWM intensities I_Y/I_X is obtained to be 6.0 for sample S3 at a delay time of 0.5 ps. In order to investigate the anisotropy of the FWM signal, we measured the angular dependence of the collinear polarization of the excitation pulses. The angular dependence of the FWM intensity, measured at a delay time of 0.5 ps, for the five samples is shown in Fig. 5. The FWM signals show strong

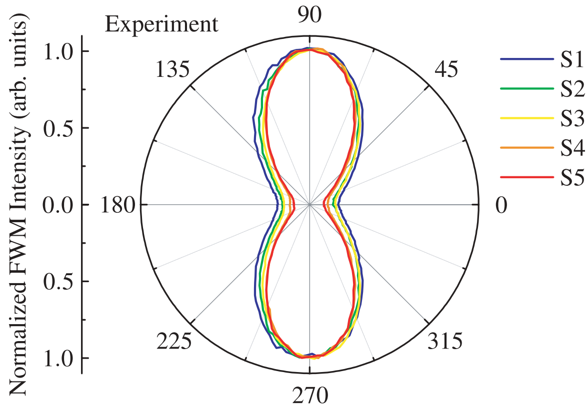

FIG. 5. (Color online) Experimental results for angular dependence of normalized four-wave mixing intensity at a delay time of 0.5 ps. The angle of linear polarization of the excitation pulse is measured from the X direction.

anisotropy with the maximum intensity at Y polarization and the minimum intensity at X polarization for all samples. Because the FWM intensity is proportional to the eighth power of the dipole moments for the exciton transitions, the anisotropic signals directly reflect the difference of the dipole moments between the X and Y excitons. It is significant that the ratio I_Y/I_X increases from 5.2 to 10.3 with increasing lattice mismatch. It clearly shows that the optical anisotropy of QDs depends on the strain due to the lattice mismatch between the QDs and spacer layers.

The observed anisotropic signals in our measurements can not be explained only by the hh excitons because linear combinations of doubly degenerated hh exciton states exhibit identical magnitudes of dipole moment. To explain the anisotropic signals obtained from highly strained QDs, the valence band mixing between the hh and lh bands should be taken into account.[9,15–17] In a quantum-confined structure, the energy of lh excitons is considerably higher than that of hh excitons due to the quantum confinement effect. Therefore, the lowest exciton level is constructed as hh-like excitons, which are the hh excitons partly mixed with lh excitons due to the strain. Because the dipole moment of lh excitons is smaller than that of hh excitons in the XY plane, the mixing causes optical anisotropy. Furthermore, the hh-like exciton states are characterized by the crystal symmetry along the X and Y directions due to the anisotropic confinement potential induced by the strain. These states show the fine-structure splitting due to the long-range electron-hole exchange interaction in QDs.

C. Theoretical treatment of exciton states in strained QDs

The valence band mixing between hh and lh bands is taken into account for the calculation of the exciton states in strained QDs. The mixing is expressed by the Bir-Pikus Hamiltonian.[23] The contribution of the split-off bands is negligible because the split-off bands are sufficiently separated from the hh and lh bands due to the spin-orbit interaction. We use the notation of $\mathrm{hh}^{\pm}$ for the hh exciton with $J_Z^{\mathrm{h}} = \pm\frac{3}{2}$ and $\mathrm{lh}^{\pm}$ for the lh exciton with $J_Z^{\mathrm{h}} = \pm\frac{1}{2}$, where J_Z^{h} denotes the Z component of the total angular momentum of the hole, which is denoted as $\boldsymbol{J}^{\mathrm{h}}$. In consequence of the valence band mixing, the exciton states are reconstructed as combinations of $\mathrm{hh}^{\pm}$ and $\mathrm{lh}^{\pm}$ excitons. As derived in Appendix A, the mixing of exciton states in the strained condition is expressed by the following Hamiltonian:

$$\mathcal{H}_{\mathrm{exciton}} = \begin{pmatrix} 0 & H & I & 0 \\ H^* & \hbar\Delta_{\mathrm{hl}} & 0 & I \\ I^* & 0 & \hbar\Delta_{\mathrm{hl}} & -H \\ 0 & I^* & -H^* & 0 \end{pmatrix} \qquad (1)$$

in the basis of (hh^+, lh^+, lh^-, hh^-) excitons. The energy difference between hh and lh excitons is denoted by $\hbar\Delta_{\mathrm{hl}}$. The mixing between hh and lh excitons is caused by the presence of the off-diagonal elements H and I, which represent the interactions that change the total angular momentum J_Z^{h} by ± 1 and ± 2, respectively. These off-diagonal elements are determined as $H = d(\varepsilon_{ZX} - i\varepsilon_{YZ})$ and $I = (\sqrt{3}b/2)(\varepsilon_{XX} - \varepsilon_{YY}) - id\varepsilon_{XY}$ with the strain tensor ε_{ij} $(i,j = X,\ Y,$ and $Z)$, where the coefficients b and d are defined as the shear deformation potentials in the growth plane. The strain H disappears in the highly symmetric growth plane, such as the (001) plane, due to one of the symmetries of the (001) plane: $\varepsilon_{ZX} = \varepsilon_{YZ} = 0$. In contrast, the symmetry of the (311) plane does not exclude the strain H. The strains H and I are restricted by $H^* = -H$ and $I^* = I$ obtained from the symmetry of the (311) plane (see Appendix A).

By diagonalizing the Hamiltonian in Eq. (1), the lowest-energy exciton states in QDs are determined as the hh-like excitons, in which the lh exciton components are partly involved due to the strain. The degenerate hh-like excitons are split into X and Y excitons due to the long-range electron-hole exchange interaction. This slight energy splitting is measured from the long-period quantum beat, i.e., the fine-structure beat, with D-polarized excitation as shown in Fig. 2(a). As derived in Appendix B, the dipole moments of the X and Y excitons are given by

$$\mu_{gX} = \frac{1}{A_-}\left\{I' - H' + \frac{1}{\sqrt{3}}\left(\sqrt{1+S^2} - 1\right)\right\}, \qquad (2)$$

$$\mu_{gY} = \frac{1}{A_-}\left\{I' + H' - \frac{1}{\sqrt{3}}\left(\sqrt{1+S^2} - 1\right)\right\} \qquad (3)$$

with

$$A_- = \sqrt{2\left(1 + S^2 - \sqrt{1+S^2}\right)}, \qquad (4)$$

where μ_{gX} and μ_{gY} denote the dimensionless dipole moments of the X and Y excitons, respectively. The dimensionless strain parameters are defined as $S^2 = |H'|^2 + I'^2$, $H' = 2H/\hbar\Delta_{\mathrm{hl}}$, and $I' = 2I/\hbar\Delta_{\mathrm{hl}}$. The magnitudes of the dipole moments depend on the strain parameters H' and I'. The anisotropic signals shown in Fig. 5 are realized by the strains under the conditions $I' < 0$ and $|H'| < |I'|$, which lead to $|\mu_{gX}| < |\mu_{gY}|$. This result shows that the strong anisotropy is mainly caused by the mixing of lh^+ (lh^-) exciton with hh^- (hh^+) exciton owing to the strain I. The anisotropic FWM signals are determined by tuning these strain parameters, which directly indicate the difference in the dipole moments.

In order to analyze the strain parameters more accurately, the biexciton contribution should be taken into account in the FWM signal. The energy structure of excitons in strained

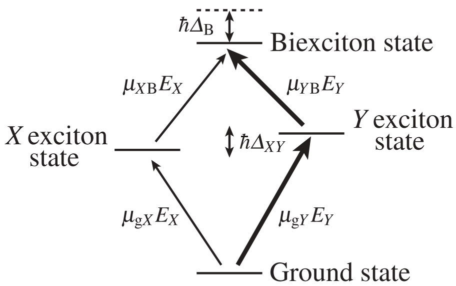

FIG. 6. Energy structure of exciton states in strained QDs. The transitions of exciton states and biexciton state are selected by the X and Y polarizations, which are denoted by E_X and E_Y. The thickness of the arrows indicates the strength of the transition.

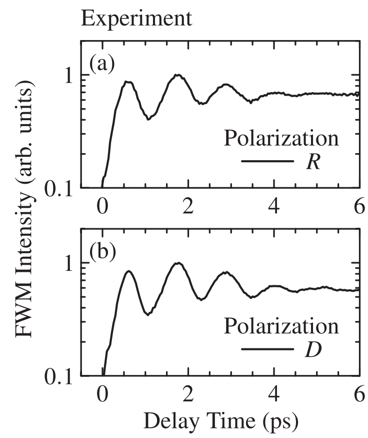

FIG. 7. Four-wave mixing intensity for sample S3 at a delay time of 0 to 6 ps with (a) R- and (b) D-polarized excitations.

QDs is shown in Fig. 6. The energy of the Y exciton state is higher than that of the X exciton state by the fine-structure splitting because the period of the exciton-biexciton beat with Y-polarized excitation is smaller than that with X-polarized excitation.[4,20] The fine-structure splitting $\hbar\Delta_{XY}$ and the biexciton binding energy $\hbar\Delta_B$ depend on the strain. The strain dependence of these values is measured from the fine-structure beat and the exciton-biexciton beat as shown in Figs. 3(a) and 4(b). The optical transitions depend on the polarization of the excitation pulses. In Fig. 6, the transition matrix elements are denoted by the light-matter interactions μE, which are the products of the dipole moment and excitation pulse, with the X-polarized (Y-polarized) electric field E_X (E_Y). The thick arrows indicate the strong transitions reflecting the optical anisotropy: $|\mu_{gX}| < |\mu_{gY}|$. The biexciton transitions also depend on the X- and Y-polarized excitations as well as the transitions of the X and Y excitons. The dipole moments of the biexciton transitions are given by $\boldsymbol{\mu}_{XB} = C\boldsymbol{\mu}_{gX}$ and $\boldsymbol{\mu}_{YB} = C\boldsymbol{\mu}_{gY}$ using the coefficient C because the beat amplitude is independent of X- and Y-polarized excitations as shown in Fig. 2(b). The coefficient C indicates the relative strength of the biexciton transition, and it was often set to a value close to 1 in previous investigations.[24–27]

The strain H plays a significant role in the exciton-biexciton beat. We measured the FWM intensity for cocircularly polarized excitation, which is denoted as R-polarized excitation. The exciton-biexciton beats with R- and D-polarized excitations are shown in Figs. 7(a) and 7(b). The suppression of biexciton excitation for cocircularly polarized excitation has been investigated in QDs grown on the (001) plane.[4,20] However, the exciton-biexciton beat is clearly observed with R-polarized excitation in our samples. The beat amplitude for R-polarized excitation completely coincides with that for D-polarized excitation as shown in Figs. 7(a) and 7(b). The same results are obtained for all samples. These amplitudes are determined by the magnitude of biexciton excitation, which are proportional to $|\mu_{Xg}^2 - \mu_{Yg}^2|$ and $|\mu_{Xg}^2 + \mu_{Yg}^2|$ for R- and D-polarized excitations, respectively (see Appendix D). If the strain H is equal to zero, $|\mu_{Xg}^2 - \mu_{Yg}^2|$ is one order of magnitude smaller than $|\mu_{Xg}^2 + \mu_{Yg}^2|$ because the dipole moments μ_{gX} and μ_{gY} become real values as determined by Eqs. (2) and (3). Due to the destructive interference between the biexciton transition from the X exciton and that from the Y exciton, the biexciton excitation is suppressed by R-polarized excitation in the highly symmetric sample with $H = 0$, which is the case in QDs grown on the (001) plane. In contrast, the strain H remains in our samples grown on the (311) plane. The result that the exciton-biexciton beats with both R- and D-polarized excitations shows an identical contrast gives us the following equation:

$$\left|\mu_{Xg}^2 - \mu_{Yg}^2\right| = \left|\mu_{Xg}^2 + \mu_{Yg}^2\right|, \tag{5}$$

which is realized owing to the presence of the purely imaginary strain H. This equation indicates the constraint between the strain parameters H' and I', i.e., H' is determined by I' through this equation as derived in Appendix D. The exciton-biexciton beat with R-polarized excitation enables us to analyze the characteristic feature of the strain H in strained QDs, which causes the partial mixing of lh^+ (lh^-) exciton with hh^+ (hh^-) exciton.

Theoretical FWM signals are treated for the four-level system shown in Fig. 6, while considering the fine-structure beat and the exciton-biexciton beat with the polarization selection rules for the X exciton, Y exciton, and biexciton. As derived in Appendix C, the angular dependence of the FWM intensity for linearly polarized excitation at a short delay time, e.g., at $\tau = 0.5$ ps, is given by

$$\begin{aligned} I(\tau,\theta) \propto |\mu_{gX}|^8 \cos^2\theta \Bigg| 2\left(\cos^2\theta + A_{XY}\frac{|\mu_{gY}|^2}{|\mu_{gX}|^2}\sin^2\theta\right) \\ - C_B e^{i\Delta_B\tau}\left(\cos^2\theta + \frac{\mu_{Yg}^2}{\mu_{Xg}^2}\sin^2\theta\right)\Bigg|^2 \\ + |\mu_{gY}|^8 \sin^2\theta \Bigg| 2\left(A_{XY}\frac{|\mu_{gX}|^2}{|\mu_{gY}|^2}\cos^2\theta + \sin^2\theta\right) \\ - C_B e^{i\Delta_B\tau}\left(\frac{\mu_{Xg}^2}{\mu_{Yg}^2}\cos^2\theta + \sin^2\theta\right)\Bigg|^2, \end{aligned} \tag{6}$$

where the phase factors of the exciton-biexciton beat $e^{i(\Delta_B \pm \Delta_{XY})\tau}$ are replaced with the factor $e^{i\Delta_B\tau}$ because the contribution of Δ_{XY} is negligible compared to that of Δ_B at a delay time of 0.5 ps. The angle θ is measured from the X direction. The magnitude of inhomogeneous broadening of the fine-structure splitting is expressed as A_{XY}, and that of the biexciton binding energy is included in the beat amplitude

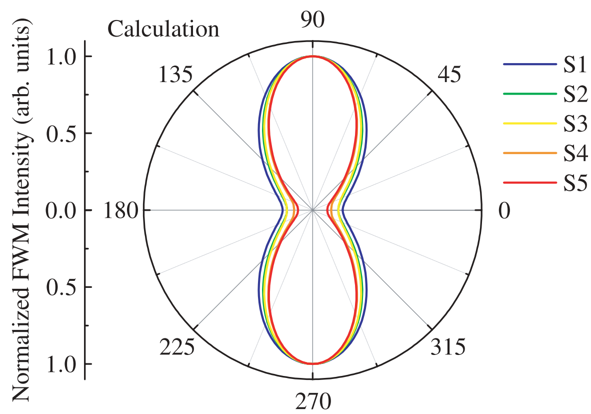

FIG. 8. (Color online) Calculated results for angular dependence of normalized four-wave mixing intensity at a delay time of 0.5 ps. The angle of linear polarization of the excitation pulse is measured from the X direction.

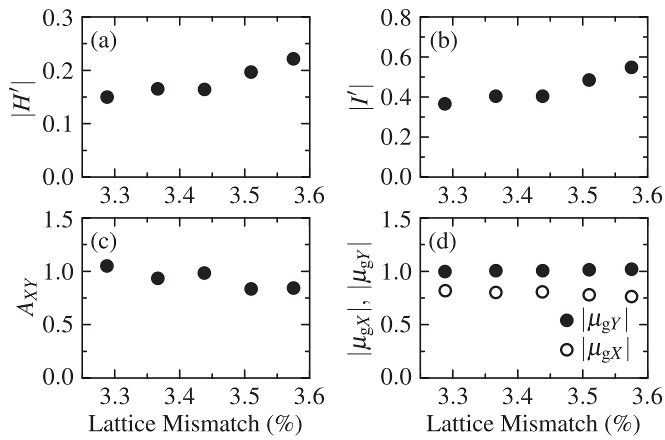

FIG. 9. Strain dependence of strain parameters (a) $|H'|$ and (b) $|I'|$, (c) magnitude of inhomogeneously broadened fine-structure splitting A_{XY}, and (d) dipole moments of X and Y excitons. The magnitudes of the dipole moments are normalized by the value $|\mu_{gY}|$ of sample S1.

C_B, which also includes the contribution of the coefficient C, as derived in Appendix C. The amplitude C_B and the angular frequency Δ_B are determined by the measurements of the exciton-biexciton beats with X- and Y-polarized excitations, as shown in Figs. 4(b) and 4(d). The dipole moments of the X and Y excitons are determined by the strain parameters H' and I' with Eqs. (2) and (3).

D. Calculated results for angular dependence of four-wave mixing intensity

The experimental data shown in Fig. 5 are fitted by Eq. (6) with the constraint of Eq. (5). The anisotropic FWM intensity is well reproduced by the calculation based on the valence band mixing due to the strain, as shown in Fig. 8. In the calculation, the only two variable parameters are H' (or I') and A_{XY} in Eq. (6). The other parameters are accurately obtained from the measurements of the exciton-biexciton beats. The calculated FWM intensity shows a maximum at Y polarization and a minimum at X polarization. The signal between these polarizations monotonically increases from the X direction to the Y direction at a delay time of 0.5 ps because of the in-phase signal in the fine-structure beat for D-polarized excitation. At long delay times, e.g., for $\tau > 100$ ps, the angular dependence shows a minimum at the direction tilted by 30° from the X direction as observed in a previous study.[28] This minimum is located at the crossover point of the signal from the X exciton with the dependence of $\cos^6\theta$ and the signal from the Y exciton with the dependence of $\sin^6\theta$ because the constructive interference due to the fine-structure beat disappears for long delay times (see Appendix C).

The variable parameters are obtained as shown in Figs. 9(a)–9(c). In the calculation, H' and I' are determined as purely imaginary and negative real values, respectively. The magnitudes of the strain parameters $|H'|$ and $|I'|$ increase with increasing lattice mismatch. This result provides evidence regarding the crucial role of spacer layers in the valence band mixing due to the strain. The exciton-biexciton beats are not suppressed by R-polarized excitation for all samples because the strain parameter H' changes depending on the strain parameter I'. The suppression of the exciton-biexciton beat due to the reduction of the strain I is canceled by the reduction of the strain H. The strain parameter I' is more than twice as strong as the strain parameter H'. It shows that optical anisotropy is mainly caused by the mixing of hh^+ (hh^-) and lh^- (lh^+) excitons due to the strain I. These hh^+ (hh^-) and lh^- (lh^+) excitons are strongly mixed with each other because both states have the up (down) spin of the hole. The magnitude of inhomogeneous broadening of the fine-structure splitting A_{XY} is nearly equal to 1.0 as shown in Fig. 9(c). The suppression of the beat amplitude A_{XY} is caused by the presence of charged excitons because charged excitons do not show the fine-structure splitting.[20] Charged excitons contribute to the partial suppression of the beat amplitude C_B in the exciton-biexciton beat. Because excitons and charged excitons are excited in different QDs, beating phenomena between these states do not occur in the FWM measurements due to the strong inhomogeneous broadening of the resonant energies. The obtained value of A_{XY} in Fig. 9(c) indicates that almost all QDs contribute to the fine-structure beat, and only a small number of charged excitons are excited. From the slight decrease in Fig. 9(c), it is found that the contribution of charged excitons to the FWM signals is increased slightly. This result corresponds to the change in the beat amplitude C_{XY} for D-polarized excitation as shown in Fig. 3(c), although C_{XY} includes the influence of the difference between the FWM intensities of the X and Y excitons. By substituting the obtained strain parameters into Eqs. (2) and (3), the dipole moments of the X and Y excitons are obtained as shown in Fig. 9(d), where the magnitudes of the dipole moments are normalized by the value $|\mu_{gY}|$ of sample S1. The magnitude of μ_{gX} slightly decreases with increasing lattice mismatch. In contrast, the magnitude of μ_{gY} shows an increasing dependence. The separation between these values is enhanced with increasing lattice mismatch because the valence band mixing between the hh and lh bands becomes stronger with increasing strain, which causes the optical anisotropy.

IV. CONCLUSION

We have investigated the strain dependence of excitons in self-assembled InAs quantum dots (QDs) grown on the (311) plane. The strain in the highly stacked QDs is controlled by tuning the lattice constant of the spacer layers. In the four-wave mixing (FWM) measurements, the fine-structure beat and the exciton-biexciton beat have been observed. These quantum beats reveal the energy structure of excitons in the strained QDs, and the energy structure is characterized by the X- and Y-polarized exciton states along the $[01\bar{1}]$ and $[\bar{2}33]$ directions, respectively. The period of the fine-structure beat becomes shorter with increasing the lattice mismatch between the QDs and spacer layers. This result shows that the fine-structure splitting is increased by the strain, which deforms the QD confinement potential. The biexciton binding energy does not show a clear dependence on the strain. For the angular-dependent measurements of linearly polarized excitation, we have observed anisotropy in the FWM intensity. This anisotropy clearly indicates the difference in the magnitudes of the dipole moments for the orthogonal X- and Y-polarized exciton states. Furthermore, the optical anisotropy between these states becomes stronger with increasing strain.

In order to understand the strain dependence of the dipole moments for excitons, we have calculated the valence band mixing between heavy-hole (hh) and light-hole (lh) bands. The hh and lh excitons are mixed due to the strains H and I, which change the Z component of the total angular momentum of the hole by ± 1 and ± 2, respectively. The anisotropic angular dependence is well reproduced by our calculation. The obtained strain parameters coincide with the increasing of the strain induced by the lattice mismatch. The difference in the dipole moments for X- and Y-polarized excitons is mainly caused by the strain I, which causes the mixing of the exciton states with the difference of ± 2 in the angular momentum. The strain H, which causes the mixing of the exciton states with the difference of ± 1 in the angular momentum, plays a significant role in the biexciton excitation for cocircularly polarized excitation. In the symmetry of the (311) plane, the presence of the strain H enables the observation of the exciton-biexciton beat with cocircularly polarized excitation. This phenomenon is a characteristic feature of QDs grown on the (311) plane because the biexciton excitation is suppressed in more symmetric samples, such as QDs grown on the (001) plane.

These studies on the anisotropic optical properties explicitly show that the control of the anisotropic exciton states in QDs can be achieved by tuning the lattice constant of the spacer layers. The strain in highly stacked QDs is conserved as the homogeneous strain due to the spacer layers, which allows us to homogenize the collective optical properties.

ACKNOWLEDGMENTS

One of the authors (H.T.) thanks Y. Arashida for useful discussions. This work was supported by the Global Center of Excellence Program by MEXT, Japan, through the Nanoscience and Quantum Physics Project of the Tokyo Institute of Technology. H.T. was supported by a Grant-in-Aid for JSPS Fellows.

APPENDIX A: EXCITON STATES IN STRAINED QUANTUM DOTS

1. Valence band mixing due to strain

For the theoretical treatment of exciton wave functions in quantum dots (QDs), we assume that the wave functions are expressed as linear combinations of electron and hole wave functions, and that the envelope functions vary slowly.[29] In this paper, the envelope functions of electrons and holes are omitted because the strain mainly affects not the envelope functions but the orbital functions. The heavy-hole (hh) and light-hole (lh) wave functions are expressed as

$$|\mathrm{hh}^+\rangle = -\frac{1}{\sqrt{2}}(P_X + iP_Y)\Uparrow, \tag{A1}$$

$$|\mathrm{lh}^+\rangle = -\frac{1}{\sqrt{6}}(P_X + iP_Y)\Downarrow + \frac{\sqrt{2}}{\sqrt{3}}P_Z\Uparrow, \tag{A2}$$

$$|\mathrm{lh}^-\rangle = \frac{1}{\sqrt{6}}(P_X - iP_Y)\Uparrow + \frac{\sqrt{2}}{\sqrt{3}}P_Z\Downarrow, \tag{A3}$$

$$|\mathrm{hh}^-\rangle = \frac{1}{\sqrt{2}}(P_X - iP_Y)\Downarrow, \tag{A4}$$

where P_j ($j = X, Y$, and Z) denotes the orbital function along the j direction, and it is defined as $P_X = (-1/\sqrt{2})(Y_1^1 - Y_1^{-1})$, $P_Y = (i/\sqrt{2})(Y_1^1 + Y_1^{-1})$, and $P_Z = Y_1^0$ with the spherical harmonics Y_l^m ($l = 1, m = \pm 1, 0$). The up (down) spin of the hole is denoted as $\Uparrow$ ($\Downarrow$). The valence band mixing due to strain is expressed by the Bir-Pikus Hamiltonian as follows:

$$\mathcal{H}_{\mathrm{hole}} = \begin{pmatrix} F & H & I & 0 \\ H^* & G & 0 & I \\ I^* & 0 & G & -H \\ 0 & I^* & -H^* & F \end{pmatrix} \tag{A5}$$

in (hh$^+$, lh$^+$, lh$^-$, hh$^-$) basis.[23] The matrix elements are given by

$$F = -a_{\mathrm{v}}\varepsilon - \frac{b}{2}(\varepsilon - 3\varepsilon_{ZZ}), \tag{A6}$$

$$G = -a_{\mathrm{v}}\varepsilon + \frac{b}{2}(\varepsilon - 3\varepsilon_{ZZ}), \tag{A7}$$

$$H = d(\varepsilon_{ZX} - i\varepsilon_{YZ}), \tag{A8}$$

$$I = \frac{\sqrt{3}b}{2}(\varepsilon_{XX} - \varepsilon_{YY}) - id\varepsilon_{XY}, \tag{A9}$$

where the coefficients a_{v}, b, and d are defined as the deformation potentials in the growth plane. The matrix elements are determined by the strain tensor ε_{ij} ($i,j = X$, Y, and Z) and $\varepsilon = \varepsilon_{XX} + \varepsilon_{YY} + \varepsilon_{ZZ}$.

Taking into account the optical selection rules of excitons, the $|\mathrm{hh}^+\rangle$ ($|\mathrm{hh}^-\rangle$) state and $|\mathrm{lh}^-\rangle$ ($|\mathrm{lh}^+\rangle$) state are coupled to the down (up) spin state of the electron as electron-hole pairs, i.e., excitons. The excitons in QDs are also influenced by the quantum confinement effect. The strain Hamiltonian for hh and lh excitons is expressed as

$$\mathcal{H}_{\text{exciton}} = \begin{pmatrix} 0 & H & I & 0 \\ H^* & \hbar\Delta_{\text{hl}} & 0 & I \\ I^* & 0 & \hbar\Delta_{\text{hl}} & -H \\ 0 & I^* & -H^* & 0 \end{pmatrix} \tag{A10}$$

in the basis of (hh^+, lh^+, lh^-, hh^-) excitons. The energy of lh excitons is separated from that of hh excitons by the energy difference $\hbar\Delta_{\text{hl}}$ due to the confinement. The off-diagonal elements due to the strain are determined by the crystal symmetry of the growth plane. In the symmetry of the (311) plane, i.e., $\varepsilon_{XY} = \varepsilon_{ZX} = 0$, the strain parameters are rewritten as

$$H = -id\varepsilon_{YZ}, \tag{A11}$$

$$I = \frac{\sqrt{3}b}{2}(\varepsilon_{XX} - \varepsilon_{YY}). \tag{A12}$$

These equations lead to the conditions $H^* = -H$ and $I^* = I$.

By diagonalizing the Hamiltonian in Eq. (A10), the eigenstates are determined as hh-like and lh-like exciton states. Using the dimensionless strain parameters defined as $S^2 = |H'|^2 + I'^2$, $H' = 2H/\hbar\Delta_{\text{hl}}$, and $I' = 2I/\hbar\Delta_{\text{hl}}$, the eigenenergies of hh-like excitons and lh-like excitons are obtained to be $\hbar\Delta_{\text{hl}}(1 - \sqrt{1+S^2})/2$ and $\hbar\Delta_{\text{hl}}(1 + \sqrt{1+S^2})/2$, respectively. The hh-like exciton states are given by

$$|\psi_{\text{h}_1}\rangle = \frac{1}{A_-}\begin{pmatrix} H' \\ 1-\sqrt{1+S^2} \\ 0 \\ I' \end{pmatrix}, \tag{A13}$$

$$|\psi_{\text{h}_2}\rangle = \frac{1}{A_-}\begin{pmatrix} I' \\ 0 \\ 1-\sqrt{1+S^2} \\ H' \end{pmatrix}, \tag{A14}$$

and the lh-like exciton states are given by

$$|\psi_{\text{l}_1}\rangle = \frac{1}{A_+}\begin{pmatrix} H' \\ 1+\sqrt{1+S^2} \\ 0 \\ I' \end{pmatrix}, \tag{A15}$$

$$|\psi_{\text{l}_2}\rangle = \frac{1}{A_+}\begin{pmatrix} I' \\ 0 \\ 1+\sqrt{1+S^2} \\ H' \end{pmatrix}. \tag{A16}$$

Here, the normalization constant $A_\pm$ is defined as

$$A_\pm = \sqrt{2\left(1 + S^2 \pm \sqrt{1+S^2}\right)}. \tag{A17}$$

We assume that the contribution of lh-like excitons to optical response is negligible because the quantum confinement effect along the Z direction is sufficiently strong in QDs. The hh-like excitons are generated as the lowest-energy exciton states in QDs by optical excitation.

2. Long-range electron-hole exchange interaction

In anisotropic QDs, these degenerate hh-like excitons are split into nondegenerate states characterized by the anisotropy of the QD confinement potential. The energy splitting between these states is determined by the long-range electron-hole exchange interaction in QDs. In our samples, these states are characterized by X- and Y-polarized excitations, which are polarized along the $[01\bar{1}]$ and $[\bar{2}33]$ directions, respectively. The energy difference between X- and Y-polarized states $\hbar\Delta_{XY}$ is quite small compared to the strain interactions, i.e., the mixing energies, between hh and lh excitons. The slight splitting $\hbar\Delta_{XY}$ has been observed as a long-period quantum beat, i.e., the fine-structure beat, in our studies. The nondegenerate X- and Y-polarized excitons are expressed as linear combinations of hh-like excitons. The X and Y excitons are obtained as follows:

$$|\psi_X\rangle = \frac{-1}{\sqrt{2}}\left(|\psi_{\text{h}_2}\rangle - |\psi_{\text{h}_1}\rangle\right), \tag{A18}$$

$$|\psi_Y\rangle = \frac{i}{\sqrt{2}}\left(|\psi_{\text{h}_2}\rangle + |\psi_{\text{h}_1}\rangle\right). \tag{A19}$$

APPENDIX B: DIPOLE MOMENTS OF EXCITON STATES AND BIEXCITON STATE

Using Eqs. (A1)–(A4), the dipole moments of hh and lh excitons are given by the following (X, Y, Z) components:

$$\langle \text{g}|\boldsymbol{p}|\text{hh}^+\rangle = \begin{pmatrix} -1/\sqrt{2} \\ -i/\sqrt{2} \\ 0 \end{pmatrix}, \quad \langle \text{g}|\boldsymbol{p}|\text{hh}^-\rangle = \begin{pmatrix} 1/\sqrt{2} \\ -i/\sqrt{2} \\ 0 \end{pmatrix}, \tag{B1}$$

$$\langle \text{g}|\boldsymbol{p}|\text{lh}^+\rangle = \begin{pmatrix} -1/\sqrt{6} \\ -i/\sqrt{6} \\ 0 \end{pmatrix}, \quad \langle \text{g}|\boldsymbol{p}|\text{lh}^-\rangle = \begin{pmatrix} 1/\sqrt{6} \\ -i/\sqrt{6} \\ 0 \end{pmatrix}, \tag{B2}$$

where $\boldsymbol{p}$ denotes the electron momentum operator; $|\text{g}\rangle$ denotes the ground state.[29] The wave functions of the electron are omitted because their contributions are eventually included in the normalization constant. Using these dipole moments, the dimensionless dipole moments of the X and Y excitons are obtained as

$$\boldsymbol{\mu}_{\text{g}X} = \langle \text{g}|\boldsymbol{p}|\psi_X\rangle = \mu_{\text{g}X}\begin{pmatrix} 1 \\ 0 \\ 0 \end{pmatrix}, \tag{B3}$$

$$\boldsymbol{\mu}_{\text{g}Y} = \langle \text{g}|\boldsymbol{p}|\psi_Y\rangle = \mu_{\text{g}Y}\begin{pmatrix} 0 \\ 1 \\ 0 \end{pmatrix} \tag{B4}$$

with

$$\mu_{\text{g}X} = \frac{1}{A_-}\left\{I' - H' + \frac{1}{\sqrt{3}}\left(\sqrt{1+S^2} - 1\right)\right\}, \tag{B5}$$

$$\mu_{\text{g}Y} = \frac{1}{A_-}\left\{I' + H' - \frac{1}{\sqrt{3}}\left(\sqrt{1+S^2} - 1\right)\right\}. \tag{B6}$$

The complex conjugate of the dipole moment is denoted by $\mu_{X\text{g}}$ ($\mu_{Y\text{g}}$), i.e., $\mu_{X\text{g}} = \mu_{\text{g}X}^*$ ($\mu_{Y\text{g}} = \mu_{\text{g}Y}^*$).

The biexciton transitions from the X and Y exciton states depend on the X- and Y-polarized excitations as shown in Fig. 6. The dipole moments of the biexciton transitions are given by

$$\boldsymbol{\mu}_{X\mathrm{B}} = C\boldsymbol{\mu}_{\mathrm{g}X}, \quad \boldsymbol{\mu}_{Y\mathrm{B}} = C\boldsymbol{\mu}_{\mathrm{g}Y}, \tag{B7}$$

where the coefficient C indicates the relative strength of the biexciton transition. It has been previously shown that the probability of the biexciton transition is nearly equal to that of the exciton transition.[24–27]

APPENDIX C: FOUR-WAVE MIXING INTENSITY FOR COLLINEARLY POLARIZED EXCITATION

The four-wave mixing (FWM) intensity is calculated by solving the optical Bloch equations up to the third order of the excitation field for a four-level system.[24,27,30,31] The excitons in QDs are modeled by four levels including the ground state, X exciton, Y exciton, and biexciton as shown in Fig. 6. The first and second excitation pulses with a delay time of τ are assumed to be delta-function pulses. The inhomogeneous broadening of the exciton resonant energy is considerably larger than the spectral linewidth of excitation pulses as shown in Fig. 1(c). The excitons contributing to the FWM signal are determined by the linewidth of the excitation pulse. Therefore, the photon echo signal also exhibits the shape of a delta function at twice the delay time. The strong inhomogeneous broadening causes the exciton-biexciton beat for positive delay times.[27] The FWM intensity for collinearly polarized excitation depends on the polarization angle of the linearly polarized pulses in the XY plane. Using the polarization angle θ measured from the X direction, the linearly polarized excitation pulse is expressed as

$$\boldsymbol{E}(\theta) = \begin{pmatrix} \cos\theta \\ \sin\theta \\ 0 \end{pmatrix}. \tag{C1}$$

The polarization selection rules are determined by the transition matrix elements $\boldsymbol{\mu}_{\mathrm{g}j}\cdot\boldsymbol{E}(\theta)$ for $j = X,Y$. The FWM intensity $I(\tau,\theta)$ is obtained as follows:

$$\begin{aligned} I(\tau,\theta) \propto{}& |\mu_{\mathrm{g}X}|^8 \cos^2\theta \bigg| 2\bigg(\cos^2\theta + f_X(\tau)\frac{|\mu_{\mathrm{g}Y}|^2}{|\mu_{\mathrm{g}X}|^2}\sin^2\theta\bigg) \\ &- h_X(\tau)\bigg(\cos^2\theta + \frac{\mu_{Y\mathrm{g}}^2}{\mu_{X\mathrm{g}}^2}\sin^2\theta\bigg)\bigg|^2 e^{-(4/T_{2X})\tau} \\ &+ |\mu_{\mathrm{g}Y}|^8 \sin^2\theta \bigg| 2\bigg(f_Y(\tau)\frac{|\mu_{\mathrm{g}X}|^2}{|\mu_{\mathrm{g}Y}|^2}\cos^2\theta + \sin^2\theta\bigg) \\ &- h_Y(\tau)\bigg(\frac{\mu_{X\mathrm{g}}^2}{\mu_{Y\mathrm{g}}^2}\cos^2\theta + \sin^2\theta\bigg)\bigg|^2 e^{-(4/T_{2Y})\tau} \end{aligned} \tag{C2}$$

with

$$f_X(\tau) = A_{XY} e^{i\Delta_{XY}\tau} e^{-(\sigma_{XY}^2/4)\tau^2}, \tag{C3}$$

$$f_Y(\tau) = A_{XY} e^{-i\Delta_{XY}\tau} e^{-(\sigma_{XY}^2/4)\tau^2}, \tag{C4}$$

$$h_X(\tau) = A_{\mathrm{B}} C^2 e^{i(\Delta_{\mathrm{B}}-\Delta_{XY})\tau} e^{-(\sigma_{\mathrm{B}}^2/4)\tau^2}, \tag{C5}$$

$$h_Y(\tau) = A_{\mathrm{B}} C^2 e^{i(\Delta_{\mathrm{B}}+\Delta_{XY})\tau} e^{-(\sigma_{\mathrm{B}}^2/4)\tau^2}, \tag{C6}$$

where the first and second terms correspond to the X- and Y-polarized signals, respectively. The fine-structure beat is expressed by the phase factor $e^{\pm i\Delta_{XY}\tau}$. The inhomogeneous broadening of the fine-structure splitting should be taken into account because the fine-structure splittings of QDs differ from each other due to the difference in the QD confinement potential. The inhomogeneous broadening is assumed to be a Gaussian distribution given by $g_{XY}(\omega) = (A_{XY}/\sqrt{\pi}\sigma_{XY})e^{-(\omega-\Delta_{XY})^2/\sigma_{XY}^2}$ with a magnitude A_{XY}, a central value $\hbar\Delta_{XY}$, and a linewidth $\hbar\sigma_{XY}$. The linewidth contributes to the damping factor $e^{-(\sigma_{XY}^2/4)\tau^2}$. For the exciton-biexciton beat, the inhomogeneous broadening of the biexciton binding energy should also be taken into account. This broadening, as well as that of the fine-structure splitting, is assumed to be a Gaussian distribution: $g_{\mathrm{B}}(\omega) = (A_{\mathrm{B}}/\sqrt{\pi}\sigma_{\mathrm{B}})e^{-(\omega-\Delta_{\mathrm{B}})^2/\sigma_{\mathrm{B}}^2}$. The exciton-biexciton beat is expressed by the phase factor $e^{i(\Delta_{\mathrm{B}}\pm\Delta_{XY})\tau}$ and the damping factor $e^{-(\sigma_{\mathrm{B}}^2/4)\tau^2}$. The dephasing times for the X and Y excitons are denoted by T_{2X} and T_{2Y}, respectively. We use the experimental result $|1/T_{2Y} - 1/T_{2X}|\tau \ll (\sigma_{XY}^2/4)\tau^2$ for simplicity. The biexciton dephasing times for the transitions to the X and Y excitons are assumed to be the same values as T_{2X} and T_{2Y}, respectively. Even if the dephasing times of the biexciton are different from those of the excitons, the difference between the dephasing times is sufficiently negligible because the damping factor $e^{-(\sigma_{\mathrm{B}}^2/4)\tau^2}$ becomes reduced much faster than the difference.

For a short delay time ($\Delta_{XY}\tau,\sigma_{XY}\tau,\sigma_{\mathrm{B}}\tau \ll 1$), the FWM signal exhibits constructive interference of the fine-structure beat between the X and Y excitons. The influence of dephasing is negligible because the dephasing times are considerably longer than the time ranges of the quantum beats. The FWM signal is rewritten as follows:

$$\begin{aligned} I(\tau,\theta) \propto{}& |\mu_{\mathrm{g}X}|^8 \cos^2\theta \bigg| 2\bigg(\cos^2\theta + A_{XY}\frac{|\mu_{\mathrm{g}Y}|^2}{|\mu_{\mathrm{g}X}|^2}\sin^2\theta\bigg) \\ &- C_{\mathrm{B}} e^{i\Delta_{\mathrm{B}}\tau}\bigg(\cos^2\theta + \frac{\mu_{Y\mathrm{g}}^2}{\mu_{X\mathrm{g}}^2}\sin^2\theta\bigg)\bigg|^2 \\ &+ |\mu_{\mathrm{g}Y}|^8 \sin^2\theta \bigg| 2\bigg(A_{XY}\frac{|\mu_{\mathrm{g}X}|^2}{|\mu_{\mathrm{g}Y}|^2}\cos^2\theta + \sin^2\theta\bigg) \\ &- C_{\mathrm{B}} e^{i\Delta_{\mathrm{B}}\tau}\bigg(\frac{\mu_{X\mathrm{g}}^2}{\mu_{Y\mathrm{g}}^2}\cos^2\theta + \sin^2\theta\bigg)\bigg|^2, \end{aligned} \tag{C7}$$

where the beat amplitude C_{B} corresponds to $A_{\mathrm{B}}C^2$. This equation is used for analyzing the anisotropic FWM intensity at a delay time of 0.5 ps.

For a long delay time ($1 \ll \sigma_{XY}\tau,\sigma_{\mathrm{B}}\tau$), the fine-structure beat and the exciton-biexciton beat disappear. The FWM intensity is rewritten as follows:

$$I(\tau,\theta) \propto |\mu_{\mathrm{g}X}|^8 \cos^6\theta e^{-(4/T_{2X})\tau} + |\mu_{\mathrm{g}Y}|^8 \sin^6\theta e^{-(4/T_{2Y})\tau}. \tag{C8}$$

We measured the angular dependence at a delay time of 150 ps, and the dependence shows four minima at $\theta = 30°$, 150°, 210°, and 330° because the signals from the X and Y excitons show the angular dependence of $\cos^6\theta$ and that of $\sin^6\theta$, respectively. If the amplitude of the signal from the X exciton coincides with that of the signal from the Y exciton, the minima are observed at $\theta = 45^\circ$, 135°, 225°, and 315°. However, the observed QDs show anisotropic intensities for the X and Y excitons, which causes a shift of the minima.

APPENDIX D: RELATION BETWEEN STRAIN PARAMETERS

The relation between the strains H and I is determined by the exciton-biexciton beats observed with cocircularly and collinearly polarized excitations. The right-circularly polarized pulse and linearly polarized pulse with $\theta = 45^\circ$, which are denoted as R- and D-polarized pulses, are expressed as

$$\boldsymbol{E}_R = \begin{pmatrix} -1/\sqrt{2} \\ -i/\sqrt{2} \\ 0 \end{pmatrix}, \quad \boldsymbol{E}_D = \begin{pmatrix} 1/\sqrt{2} \\ 1/\sqrt{2} \\ 0 \end{pmatrix}, \tag{D1}$$

respectively. For j-polarized excitation ($j = R,D$), the excitation probability of biexciton is expressed as $|(\boldsymbol{\mu}_{BX}\cdot\boldsymbol{E}_j)(\boldsymbol{\mu}_{Xg}\cdot\boldsymbol{E}_j) + (\boldsymbol{\mu}_{BY}\cdot\boldsymbol{E}_j)(\boldsymbol{\mu}_{Yg}\cdot\boldsymbol{E}_j)|^2$. In our experiment, the FWM signals exhibit the equally strong exciton-biexciton beats for both R- and D-polarized excitations as shown in Figs. 7(a) and 7(b). This result shows that the biexciton excitation does not change for these polarized excitations. Using the expression of R- and D-polarized excitations in Eq. (D1), this result is expressed as follows:

$$\left|\mu_{Xg}^2 - \mu_{Yg}^2\right|^2 = \left|\mu_{Xg}^2 + \mu_{Yg}^2\right|^2, \tag{D2}$$

where we use Eq. (B7) for the dipole moments of the biexciton. The left- and right-hand sides correspond to the excitation probabilities of biexcitons for R- and D-polarized excitations, respectively. By substituting Eqs. (B5) and (B6) into this equation, the relation between the strain parameters is obtained as

$$\left\{I'^2 - |H'|^2 - \frac{1}{3}\left(\sqrt{1+S^2} - 1\right)^2\right\}^2 - 4I'^2|H'|^2 = 0, \tag{D3}$$

where $S^2 = |H'|^2 + I'^2$. The strain parameters $|H'|$ and I' are determined with satisfying this equation.

[1] J. A. Gupta, D. D. Awschalom, X. Peng, and A. P. Alivisatos, Phys. Rev. B **59**, R10421 (1999).
[2] M. V. Gurudev Dutt, J. Cheng, B. Li, X. Xu, X. Li, P. R. Berman, D. G. Steel, A. S. Bracker, D. Gammon, S. E. Economou, R.-B. Liu, and L. J. Sham, Phys. Rev. Lett. **94**, 227403 (2005).
[3] P. Borri, W. Langbein, S. Schneider, U. Woggon, R. L. Sellin, D. Ouyang, and D. Bimberg, Phys. Rev. Lett. **87**, 157401 (2001).
[4] W. Langbein, P. Borri, U. Woggon, V. Stavarache, D. Reuter, and A. D. Wieck, Phys. Rev. B **70**, 033301 (2004).
[5] J. Ishi-Hayase, K. Akahane, N. Yamamoto, M. Sasaki, M. Kujiraoka, and K. Ema, Appl. Phys. Lett. **91**, 103111 (2007).
[6] J. J. Finley, P. W. Fry, A. D. Ashmore, A. Lemaître, A. I. Tartakovskii, R. Oulton, D. J. Mowbray, M. S. Skolnick, M. Hopkinson, P. D. Buckle, and P. A. Maksym, Phys. Rev. B **63**, 161305(R) (2001).
[7] E. Poem, J. Shemesh, I. Marderfeld, D. Galushko, N. Akopian, D. Gershoni, B. D. Gerardot, A. Badolato, and P. M. Petroff, Phys. Rev. B **76**, 235304 (2007).
[8] Y. Arashida, Y. Ogawa, and F. Minami, Phys. Rev. B **85**, 235318 (2012).
[9] L.-W. Wang, J. Kim, and A. Zunger, Phys. Rev. B **59**, 5678 (1999).
[10] O. Stier, M. Grundmann, and D. Bimberg, Phys. Rev. B **59**, 5688 (1999).
[11] L. Besombes, K. Kheng, and D. Martrou, Phys. Rev. Lett. **85**, 425 (2000).
[12] R. Seguin, A. Schliwa, S. Rodt, K. Pötschke, U. W. Pohl, and D. Bimberg, Phys. Rev. Lett. **95**, 257402 (2005).
[13] G. A. Narvaez, G. Bester, and A. Zunger, Phys. Rev. B **72**, 245318 (2005).
[14] A. Schliwa, M. Winkelnkemper, and D. Bimberg, Phys. Rev. B **79**, 075443 (2009).
[15] A. V. Koudinov, I. A. Akimov, Y. G. Kusrayev, and F. Henneberger, Phys. Rev. B **70**, 241305(R) (2004).
[16] D. N. Krizhanovskii, A. Ebbens, A. I. Tartakovskii, F. Pulizzi, T. Wright, M. S. Skolnick, and M. Hopkinson, Phys. Rev. B **72**, 161312(R) (2005).
[17] Y. Léger, L. Besombes, L. Maingault, and H. Mariette, Phys. Rev. B **76**, 045331 (2007).
[18] K. Akahane, N. Ohtani, Y. Okada, and M. Kawabe, J. Cryst. Growth **245**, 31 (2002).
[19] K. Akahane, N. Yamamoto, and T. Kawanishi, Phys. Status Solidi A **208**, 425 (2011).
[20] W. Langbein, P. Borri, U. Woggon, V. Stavarache, D. Reuter, and A. D. Wieck, Phys. Rev. B **69**, 161301(R) (2004).
[21] D. Gammon, E. S. Snow, B. V. Shanabrook, D. S. Katzer, and D. Park, Phys. Rev. Lett. **76**, 3005 (1996).
[22] M. Bayer, G. Ortner, O. Stern, A. Kuther, A. A. Gorbunov, A. Forchel, P. Hawrylak, S. Fafard, K. Hinzer, T. L. Reinecke, S. N. Walck, J. P. Reithmaier, F. Klopf, and F. Schäfer, Phys. Rev. B **65**, 195315 (2002).
[23] E. L. Ivchenko and G. E. Pikus, *Superlattices and Other Heterostructures: Symmetry and Optical Phenomena* (Springer, Berlin, 1997).
[24] K. Bott, O. Heller, D. Bennhardt, S. T. Cundiff, P. Thomas, E. J. Mayer, G. O. Smith, R. Eccleston, J. Kuhl, and K. Ploog, Phys. Rev. B **48**, 17418 (1993).
[25] A. E. Paul, J. A. Bolger, A. L. Smirl, and J. G. Pellegrino, J. Opt. Soc. Am. B **13**, 1016 (1996).
[26] H. P. Wagner, A. Schätz, W. Langbein, J. M. Hvam, and A. L. Smirl, Phys. Rev. B **60**, 4454 (1999).
[27] T. F. Albrecht, K. Bott, T. Meier, A. Schulze, M. Koch, S. T. Cundiff, J. Feldmann, W. Stolz, P. Thomas, S. W. Koch, and E. O. Göbel, Phys. Rev. B **54**, 4436 (1996).
[28] J. Ishi-Hayase, K. Akahane, N. Yamamoto, M. Kujiraoka, K. Ema, and M. Sasaki, Phys. Status Solidi C **6**, 162 (2009).
[29] P. Y. Yu and M. Cardona, *Fundamentals of Semiconductors: Physics and Material Properties* (Springer, Berlin, 2010).
[30] T. Yajima and Y. Taira, J. Phys. Soc. Jpn. **47**, 1620 (1979).
[31] E. J. Mayer, G. O. Smith, V. Heuckeroth, J. Kuhl, K. Bott, A. Schulze, T. Meier, D. Bennhardt, S. W. Koch, P. Thomas, R. Hey, and K. Ploog, Phys. Rev. B **50**, 14730 (1994).